ACS APPLIED NANO MATERIALS

www.acsanm.org
Article

Reduced Graphene Oxide-Coated Fabrics for Joule-Heating and Antibacterial Applications

Behnaz Jafari and Gerardine G. Botte*

Cite This: ACS Appl. Nano Mater. 2023, 6, 20006−20017
Read Online

ACCESS | Metrics & More | Article Recommendations | Supporting Information

ABSTRACT: Multifunctional textiles have emerged as a significant area of research due to their growing importance and diverse applications. The main requirement for these fabrics is electroconductivity, which is usually gained by incorporating conductive materials such as graphene into the textile structure. In this article, an electrochemical method was demonstrated to integrate different loadings of reduced graphene oxide (rGO) into fabrics for enhanced electrical conductivity. The process involves spray coating of graphene oxide (GO) onto the fabric, followed by in situ electrochemical reduction of GO, resulting in a coating layer of rGO nanosheets. The rGO-coated fabric exhibited exceptional Joule-heating capabilities, achieving 127 °C under a 9 V direct voltage with only 770 $\mu g/cm^2$ of rGO loading. Moreover, the antibacterial properties of the rGO-coated fabric were demonstrated, showing a significant reduction rate of over 99.99% against both *Bacillus subtilis* and *Escherichia coli*. Joule-heating and antibacterial performances of the rGO-coated fabric were investigated over eight repeated cycles, demonstrating excellent repeatability. The simplicity of the fabrication method, along with the electrothermal and antibacterial effects of the rGO-coated fabric, makes it a promising material for various practical applications.

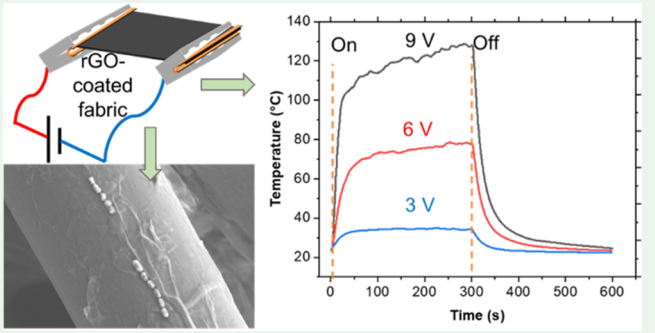

KEYWORDS: *antibacterial, conductive fabric, graphene, Joule heating, smart textile*

INTRODUCTION

Smart multifunctional textiles have drawn tremendous interest because of their potential applications in the fields of healthcare, Joule heaters, wearable sensors, and motion detectors.[1−3] A critical requirement for smart textiles is electrical conductivity.[4] However, textile substrates are inherently electrically insulated, making them unsuitable for use in electronic devices. Therefore, the main challenge in developing multifunctional textiles lies in successfully integrating electrical conductivity into the fabrics.[5,6] Graphene-based materials have been proposed as one of the ideal conductive materials to be incorporated into textiles to obtain electrical conductivity.[7]

Graphene has gained growing attention over the past few years because of its unique properties. This honeycomb-shaped two-dimensional material with an sp^2 carbon structure possesses superior electrical and thermal conductivity, robust mechanical strength, and large surface-active sites.[8,9] Furthermore, graphene materials offer antimicrobial properties through a combination of membrane stress, generation of oxidative stress, trapping effect, and photothermal activity.[10,11] However, it should be noted that graphene and its derivatives typically require a prolonged exposure time to effectively kill or inactivate microorganisms through these mechanisms.[12] It has been suggested that the application of electricity can accelerate and enhance microbial inactivation on conductive surfaces through various mechanisms such as direct electron transfer, oxidative stress, and Joule heating.[13] Joule heating happens when an electric current passes a conductor with enough resistance to convert electrical energy to thermal energy.[14]

Textiles with integrated electrical conductivity can efficiently utilize the Joule-heating effect for thermal treatment, offering a viable solution for sterilization. Thermal treatment of pathogens is a promising technology for sterilization due to its rapid and pollutant-free operation.[15] Joule heaters offer an alternative to energy-intensive and nonportable heating methods like ovens or autoclaves for disinfection. The electrothermal technique enables localized heating, reduces energy consumption, and offers portability while still ensuring effective disinfection with shorter contact times.

Several studies have reported different methods to incorporate graphene materials into textiles for the preparation of electrothermal heaters. For instance, Hao et al. reported the

Received: August 16, 2023
Accepted: September 27, 2023
Published: October 16, 2023

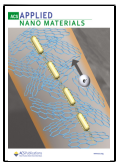

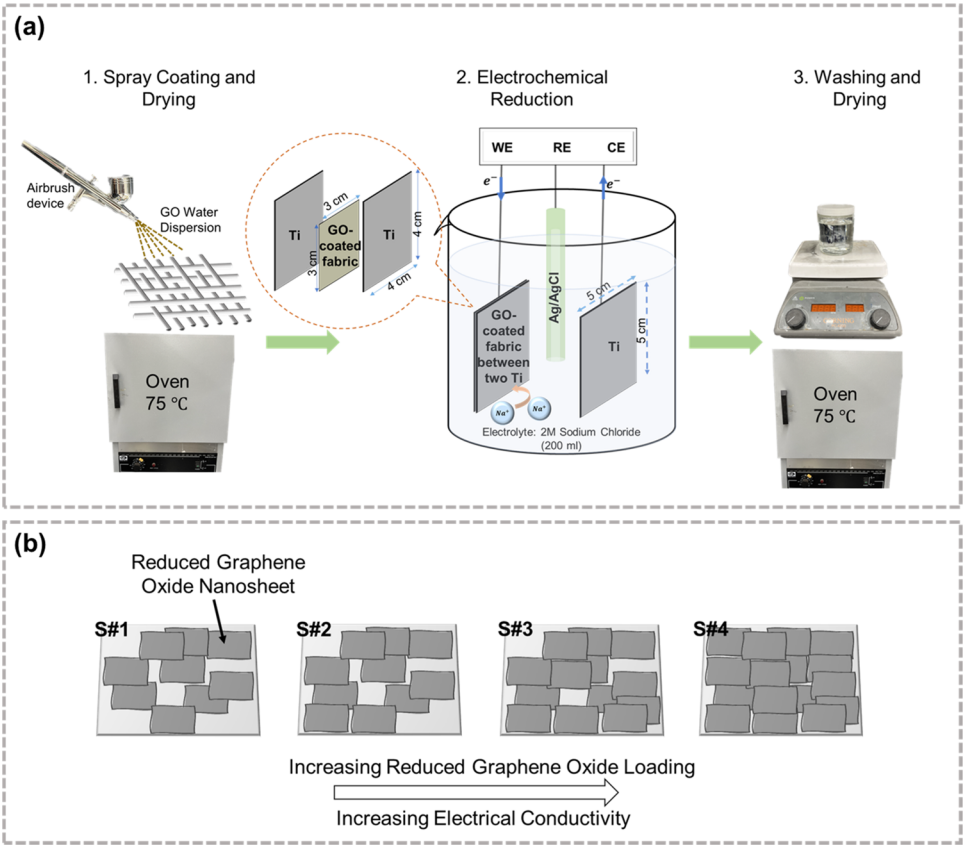

Figure 1. (a) Schematic view of the preparation procedure of the rGO-coated fabrics. (b) Schematic illustration of the repeating coating process on the fabric.

fabrication of abrasion-resistant graphene/tourmaline fabrics via a spray coating route. In this method, the modified fabrics were prepared for Joule-heating application through a sequential spray coating of water-soluble polyurethane (WPU), tourmaline/graphene/WPU ink, and another layer of WPU. By applying a voltage of 10 V, a steady-state temperature of 75.4 °C was achieved within 30 s for the fabricated Joule heater.[16] In another study, conductive fabrics were created by applying graphene onto the textile substrate using a knife-coating technique.[17] In this method, a coating paste consisting of a thickener, binder, fixing agent, ammonia, distilled water, and graphene nanoplatelets was prepared and then knife-coated onto the fabric samples. The study reported achieving temperatures of up to 100 °C under 40 V. Jain and Chatterjee developed graphene-functionalized fabrics for thermotherapy applications. The process involved dip coating of GO into the fabric, followed by chemical reduction using a sodium dithionite as a reducing agent, resulting in rGO.[18] The modified fabric exhibited a maximum temperature of 118 °C under a direct voltage of 30 V.

These studies provide evidence of the successful Joule-heating performance of graphene-coated fabrics. However, these methods involve multiple steps, various reagents, and high voltages to achieve elevated temperatures. Therefore, it is crucial to explore simpler techniques for preparing graphene-coated fabrics that exhibit high temperatures under low voltages, ensuring both human safety and energy efficiency.

In this paper, the reduced graphene oxide-coated fabrics were prepared using a facile in situ procedure developed by Jafari et al.[19] In this method, the fabrics were first spray-coated with a graphene oxide water dispersion. Spray coating is a simple method that creates an even coating layer on the fabric and can be used for textiles with uneven structures.[20] Following the spray coating step, the GO layer on the fabric was reduced electrochemically to rGO using a three-electrode system. The reduction of GO to produce rGO is a cost-effective approach for large-scale graphene production.[21] Additionally, the electrochemical reduction route is advantageous, as it does not require the use of toxic reducing agents. To study the influence of rGO loading on fabric electrical conductivity and Joule-heating performance, the fabrics were coated with varying levels of rGO. Characterization techniques, including Raman spectroscopy, scanning electron microscopy (SEM), and thermogravimetric analysis (TGA), were employed to assess the coated fabrics. The fabric demonstrating the most favorable Joule-heating performance was chosen for subsequent antibacterial testing under an electric field. The obtained results are comprehensively presented and discussed in this paper.

MATERIALS AND METHODS

Materials. Nonwoven fabrics, consisting of 50% rayon and 50% polyester, were supplied by Grainger (Manufacturer: Berkshire, model no PWAP12.24, made in Taiwan) and utilized as the substrate for the preparation of the modified fabrics. Agar powder (CAS 9002−18−0) and sodium chloride (NaCl, assay 99.0%, CAS 7647−14−5−003) were purchased from Fisher Scientific. Ultrapure Milli-Q DI water was employed for all experiments conducted. Titanium (Ti) wires of 1 mm diameter (99.99% metals basis, CAS 7440−32−6,) and Ti foils of 0.5 mm thickness (99.99% metals basis, CAS 7440−32−6) from Alfa Aesar were used as the current collectors and electrodes. Monolayer

https://doi.org/10.1021/acsanm.3c03825
ACS Appl. Nano Mater. 2023, 6, 20006−20017

graphene oxide water dispersion (4 mg/mL) was purchased from MSE Supplies for the preparation of graphene-coated fabrics. Luria−Bertani broth (Lennox) was supplied by Sigma-Aldrich. Poly(tetrafluoroethylene) (PTFE) film tape (model #1/2−36−5480) with silicone adhesive side was supplied by Grainger. A silver/silver chloride (Ag/AgCl) electrode from Koslow Scientific was used as the reference electrode in the electrochemical experiments. A copper (Cu) foil with a thickness of 0.254 mm was supplied by Grainger (manufacturer model: 4UGT2, CAS 7440−50−8).

Equipment. A SUNKKO 737G+ welding machine (pulse: 1, current: 30) was used to spot-weld the Ti wires to Ti foils. A Gamry potentiostat (Interface 1010E) was utilized to conduct the electrochemical steps of the procedure. The samples, when necessary, were dried using a Quincy Lab model 30 Lab Oven. The graphene-coated fabrics were characterized by using a Bruker Optics Senterra dispersive Raman microscope spectrometer. In addition, the morphology of the fabrics was observed using a Hitachi S-4700 field emission scanning electron microscope (FE-SEM). Thermogravimetric analysis (TGA, STAPT 1600, Linseis) was used for the thermal analysis of the samples. The resistance of the fabrics was assessed using a four-point probe method and a Keithley 2400 source meter manufactured by Tektronix. A DANOPLUS thermometer data logger with a k-type thermocouple probe with a measuring range from −50 to 300 °C and accuracy of 1.5% was used to measure and record the temperature of the fabrics. A TekPower TP5003T direct current power supply was used for applying the voltage to the rGO-coated fabrics during the experiments. The bacterial culture was incubated in a Fisherbrand Isotemp incubator using a Fisherbrand orbital shaker (both from Fisher Scientific). The optical density (OD) of the bacteria culture was measured by using a BioTek Synergy HT microplate reader. The morphology of the bacteria cells on the fabrics was investigated using a Zeiss cross-beam 540 scanning electron microscope.

Preparation Procedure of rGO-Coated Fabrics. The preparation procedure of rGO-coated fabrics was detailed in our previous study.[19] However, slight modifications were made to accommodate the coating of larger fabrics with a higher graphene loading. The procedure is shown in Figure 1(a) and described next.

In the first step, 530 μL of GO dispersion (4 mg/mL) was spray-coated on one side of the 3 cm × 3 cm rayon/polyester fabric. This was performed using a Master airbrush sprayer model G233 and compressed nitrogen gas at 15 psi pressure (ultrahigh purity, Praxair). Afterward, the GO-coated fabric was placed in a glass Petri dish and transferred to an oven with a temperature of 75 °C. The fabric was allowed to dry for a duration of 10 min under these conditions. Next, the other side of the fabric was spray-coated and dried using a similar procedure. Coating and drying each side separately were employed to minimize the loss of graphene oxide.

Next, the GO-coated fabric was sandwiched between two Ti foils each 4 cm × 4 cm. Two Ti foils were held together by using PTFE tape and were connected to a Gamry potentiostat as the working electrode (WE). A Ti foil (5 cm × 5 cm) and Ag/AgCl were used as the counter electrode (CE) and the reference electrode (RE), respectively. The electrodes were placed in a 250 mL beaker. The distance between the WE and CE was kept at 1 cm in all experiments. 200 mL of 2 M NaCl was added to the beaker as the electrolyte for the electrochemical reduction of GO. The concentration of the electrolyte was increased compared to our previously reported methodology due to the larger graphene loading and higher electrode surface area. This higher concentration of ions ensures that the electrolyte does not limit the reactions. To electrochemically reduce GO, a chronoamperometry step was performed at a potential of −1.4 V vs Ag/AgCl for a duration of 1h. The electrolyte was not stirred, and the reduction took place under ambient room conditions. After completion, the fabric was submerged in DI water and stirred for 10 min at 100 rpm to eliminate the NaCl salt adhering to the fibers. Subsequently, the fabric was placed in an oven at 75 °C for 10 min to dry.

To enhance the rGO loading on the fabric, an iteration of the coating was performed, which includes steps 1 through 3 as depicted in Figure 1(a). Four distinct samples with varying levels of rGO loading, denoted as S#1, S#2, S#3, and S#4, were prepared, corresponding to coating iterations 1, 2, 3, and 4, respectively. The purpose was to investigate the influence of loading on the electrical conductivity and Joule-heating performance. This iterative process of spray coating and electrochemical reduction ensures improved adherence of rGO nanosheets to the fabric and promotes a more thorough electrochemical reduction, resulting in an enhanced electrical conductivity and performance of the rGO-coated fabric.

To obtain the rGO loading, the fabrics were weighed before and after the desired number of iterations. The equation below was used to calculate the rGO loading of the fabric

$$\text{rGO loading} = \frac{W_2 - W_1}{A} \tag{1}$$

where W_1 is the initial weight of fabric without any coating, W_2 is the weight after completion of the coating process, and A represents the surface area of the fabric, measuring 3 cm × 3 cm.

Samples were divided into four segments of equal size (1.5 cm × 1.5 cm) for subsequent Joule-heating and antibacterial experiments.

Characterization. The Raman spectra of the rGO-coated fabrics were measured using a Bruker Optics Senterra dispersive Raman microscope spectrometer with a spectral resolution of 3−5 cm^{-1}, using a 20× microscope objective and 532 nm laser excitation. To examine the morphology of the fabric samples using FE-SEM, the fabrics were initially sputter-coated with iridium. Subsequently, they were positioned on carbon tape and mounted onto an SEM specimen stub. The SEM images were captured with a working distance of 6 mm and an accelerating voltage of 2 kV. TGA of the fabrics was performed under a nitrogen environment with a purity of 99.99% (provided by Airgas). The nitrogen was supplied at a flow rate of 50 mL/min during the experiment. The TGA analysis was conducted by raising the temperature from 25 to 600 °C with a ramp rate of 20 °C/min. The morphology of the bacteria cells on the sample fabrics was visualized via SEM imaging; the preparation procedure of the samples is described in the Supporting Information.

Electrothermal Experiments. Figure 4(a) depicts a schematic representation of the fabric's connection to the power supply and thermometer for investigating its electrothermal performance. Cu foils and alligator clips were utilized to connect the 1.5 cm × 1.5 cm rGO-coated fabric to the power supply (actual photograph shown in Figure S1). Additional information about the experimental setup can be found in the Supporting Information.

The power supply provided a current reading for each applied voltage with a resolution of 1 mA. To measure the temperature of the fabric, the thermocouple was directly attached to the center of the rGO-coated fabric by using PTFE tape. The temperature profile was measured on a per-second basis and recorded on a laptop connected to the thermometer.

Antibacterial Experiments. Antibacterial tests were conducted using *Bacillus subtilis* (ATCC 6633), a Gram-positive bacterium, and *Escherichia coli* (ATCC 11303), a Gram-negative bacterium. The AATCC 100:2004 method was employed to investigate the antibacterial activity of the rGO-coated fabrics. The preparation procedure for the *B. subtilis* test inoculum is described below while the preparation details for the *E. coli* test inoculum is provided in the Supporting Information.

A single colony of *B. subtilis* was suspended in 20 mL of sterile Luria−Bertani (LB) broth in an Erlenmeyer flask. The flask was then incubated at 37 °C while shaking at 200 rpm for a period of 18−24 h. Next, 300 μL of the *B. subtilis* culture, which had been incubated for 18−24 h, was transferred to 20 mL of sterile LB broth. After around 2.5 h of incubation at 37 °C and shaking at 200 rpm, the OD at 600 nm (OD_{600}) of the *B. subtilis* culture was measured and found to be between 0.6 and 0.7 corresponding to a cell concentration of 3×10^8 to 5×10^8 cells/mL. The test inoculum was prepared by diluting the 2.5 h culture to achieve a cell concentration range of 2×10^6 to 4×10^6 cells/mL.

In the next step, a volume of 60 μL of the prepared test inoculum was dropped onto an agar plate. Then, the 1.5 cm × 1.5 cm rGO-

https://doi.org/10.1021/acsanm.3c03825
ACS Appl. Nano Mater. 2023, 6, 20006−20017

coated fabric was placed on top of the inoculum for a period of 40 s to allow for absorption. To apply an electric field, the inoculated rGO-coated fabric was connected to a direct current (DC) power supply by using the method described in the preceding section. This allowed for the application of the desired electric field and exposure time to the fabric and the bacteria present on its surface. Following this, each sample was transferred to a tube containing 2 mL of LB broth and subjected to vortexing for 30 s to release the cells into the solution. The solution was then serially diluted to perform the plate count method, enabling the quantification of the viable cells present on each fabric.

A control sample was prepared by inoculating a piece of 1.5 cm × 1.5 cm raw fabric with the bacteria, following a procedure similar to that used for the rGO-coated fabric. The control sample was promptly transferred to a tube containing 2 mL of LB broth after inoculation and vortexed to prepare it for the plate count method.

The reduction rate ($R\%$) for the rGO-coated fabrics was calculated based on the equation below

$$R\% = \frac{(B - A)}{B} \times 100 \tag{2}$$

Here, B represents the number of colonies recovered from the control immediately after inoculation and A corresponds to the number of colonies recovered from the rGO-coated fabric after the application of a specific current and exposure time.

RESULTS AND DISCUSSION

Characterization of rGO-Coated Fabrics. Four samples with different levels of rGO were prepared through multiple coating iterations to investigate the effect of rGO loading on the electrical and electrothermal performances. A pristine fabric with zero rGO loading was used as a control for the experiments. The resistance ($R = V/I$) of each sample was measured following the 4-point method. These R values were then used to calculate the electrical conductivity (σ) of each sample using eq 3

$$\sigma = (k \cdot R \cdot t)^{-1} \tag{3}$$

where k is a geometric correction factor, which is equal to 3.48 for rectangular samples with 1.5 cm by 1.5 cm dimensions,[22] and t represents the sample thickness, which is assumed to be consistent at 0.2 mm for all samples.

Table 1 illustrates the values of the electrical conductivity, resistance, and rGO loading of fabrics with different coating iterations. Based on the presented results, it can be inferred that as the number of iterations increased, the rate of weight change on the fabric gradually slowed down. One possible explanation is that the attaching groups on the fabric became saturated, making them unable to accommodate further coating.

Table 1. Samples with Different rGO Loadings and Their Corresponding Resistance and Electrical Conductivity

sample	rGO loading, $\mu g/cm^2$	resistance, Ω	electrical conductivity, S/m
control	0	∞	0
S#1	288 ± 15	114 ± 6	13 ± 1
S#2	533 ± 16	32 ± 1	45 ± 1
S#3	655 ± 27	22 ± 2	65 ± 5
S#4	770 ± 19	11 ± 1	134 ± 6

The pristine fabric is an insulating material with no inherent conductivity. However, through successive coating iterations, the rGO level increases, leading to a corresponding increase in the electrical conductivity of the fabric. The electrical conductivity of S#4 is approximately 1 order of magnitude higher than other samples; therefore, S#4 was expected to exhibit superior electrical and electrothermal behavior compared to the rest.

Figure 1(b) schematically illustrates the potential effect of increasing the rGO loading on the formation of a more continuous graphene network with an increased number of connection points between graphene nanosheets. This structural transformation results in improved electron mobility and higher electrical conductivity due to a more favorable pathway for electron flow.

The Raman spectra of the rGO-coated fabrics with different loading levels are presented in Figure 2(a). The results reveal the presence of two prominent peaks in each sample's Raman spectrum. The D band, located at approximately 1340 cm^{-1} corresponds to structural defects, while the G band observed around 1580 cm^{-1} is related to the C=C stretching vibration of sp^2-bonded carbon atoms. These distinct peaks confirm the presence of graphene nanosheets in the fabrics. Furthermore, the intensity of D (I_D) is slightly greater than the intensity of G (I_G) for all samples which can be attributed to the removal of the oxygen functional groups during the reduction process.[23]

The surface morphologies of the samples with different rGO loadings are shown in Figure 3. As expected, an increase in rGO loading on the fabric promotes interconnections between graphene nanosheets by effectively covering a larger surface area of the fabric. This explanation is supported by the SEM images of the control, S#1, S#2, S#3, and S#4 samples. The first column of Figure 3, captured at low magnification, provides a comprehensive overview of the fabrics. These images reveal that as the loading of rGO increased, a larger portion of the fabric's surface was coated with rGO nanosheets. Consequently, this phenomenon resulted in the creation of an improved pathway for electrons within the fabric, facilitating an enhanced electron transport. At higher magnification, the SEM images reveal the presence of wrinkles caused by the rGO nanosheets in all samples except for the control sample.

TGA was conducted to examine the impact of the rGO content on the thermal resistance of the fabric. The TGA results of the control, S#1, S#2, S#3, and S#4 are depicted in Figure 2(b), presenting the residual weight percentage as a function of temperature.

All samples demonstrated an initial minor weight loss primarily attributed to the vaporization of moisture.[24] In addition, all of the samples exhibited two dramatic weight losses that could be due to the presence of two polymers, namely, rayon and polyester. Previous studies have reported that rayon decomposition starts at temperature around 200 °C,[25] while decomposition of polyester begins approximately at 360 °C.[26] The characteristics of the thermal decompositions observed in the samples are summarized in Table 2. Notably, the incorporation of rGO into the fabric led to a shift in the decomposition temperatures to higher values and a delay in the degradation.[27] The magnitude of this shift increased with higher rGO loading, indicating a direct correlation between the rGO loading and the extent to which the decomposition temperatures are elevated. Moreover, an increase in rGO content is associated with a higher weight residue, suggesting that rGO contributes to the formation of a greater amount of solid residues during the decomposition process. These observations suggests that the presence of rGO contributes to improved resistance against thermal degradation.[28,29]

https://doi.org/10.1021/acsanm.3c03825
ACS Appl. Nano Mater. 2023, 6, 20006−20017

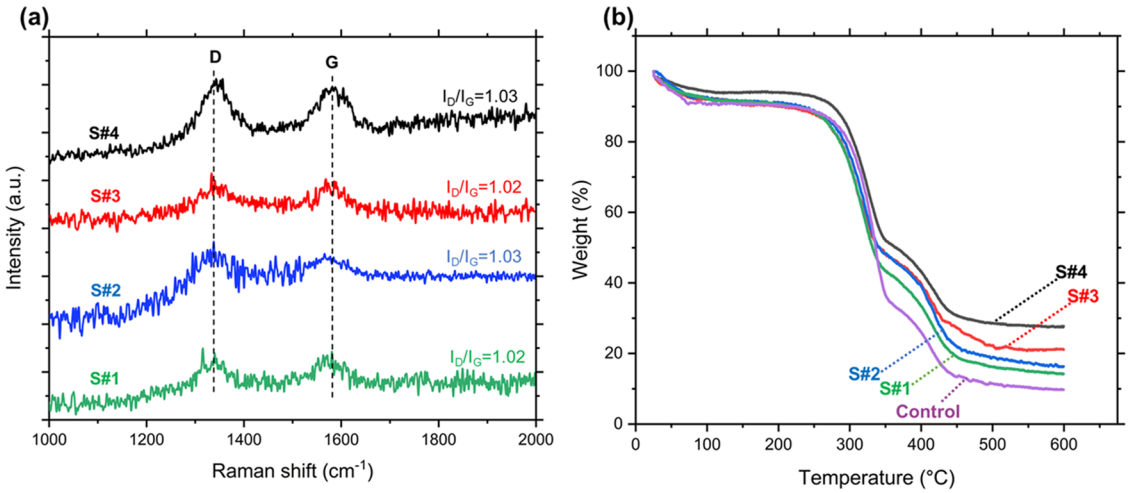

Figure 2. (a) Raman spectra of samples S#1, S#2, S#3, and S#4. (b) TGA curves of control, S#1, S#2, S#3, and S#4.

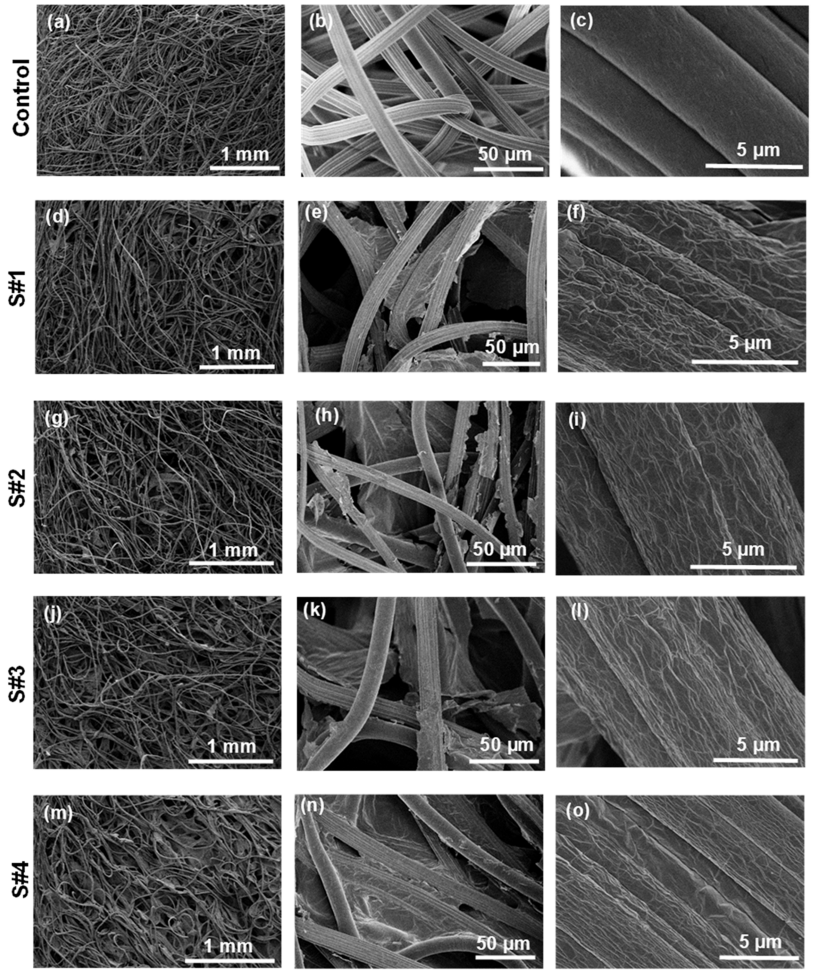

Figure 3. SEM images of control (a–c), S#1 (d–f), S#2 (g–i), S#3 (j–l), and S#4 (m–o). Wrinkled surfaces are created by the rGO nanosheets on the rGO-coated fabrics, contrasting with the smooth surface observed in the control sample.

Electrothermal Performance. The voltage–current (V–I) behavior of samples with varying rGO loads was investigated. Different DC voltages were applied to each fabric by using the power supply, and the resulting currents were recorded. Figure 4(b) presents the V–I curves for each sample. As previously mentioned, the electrical conductivity of S#4 is approximately 1 order of magnitude higher than that of the other samples. Therefore, it exhibited a significantly more robust current response compared with all of the other samples. Conversely, S#1, which underwent only one coating iteration, exhibited relatively poor current responses.

The Joule-heating performance of the fabrics was investigated by measuring their surface temperatures under different applied voltages. The results of this evaluation are presented in

https://doi.org/10.1021/acsanm.3c03825
ACS Appl. Nano Mater. 2023, 6, 20006–20017

Table 2. Thermal Decomposition Characteristics of Samples with Different Amounts of rGO

	1st main decomposition stage			2nd main decomposition stage			
sample	T_i[a]	T_f[a]	weight loss, %	T_i[a]	T_f[a]	weight loss, %	residual weight, %
control	209	351.4	55.5	378	460.7	18.2	9.77
S#1	211.7	352.3	47.8	383	453.7	19	14.1
S#2	211	345	43.4	388.7	454.6	20.2	16.4
S#3	212.5	346	41	391.1	463.3	18.8	21.3
S#4	224.2	348	41.5	393	451.8	15.5	27.7

[a] T_i and T_f are the initial and final temperatures (°C), respectively.

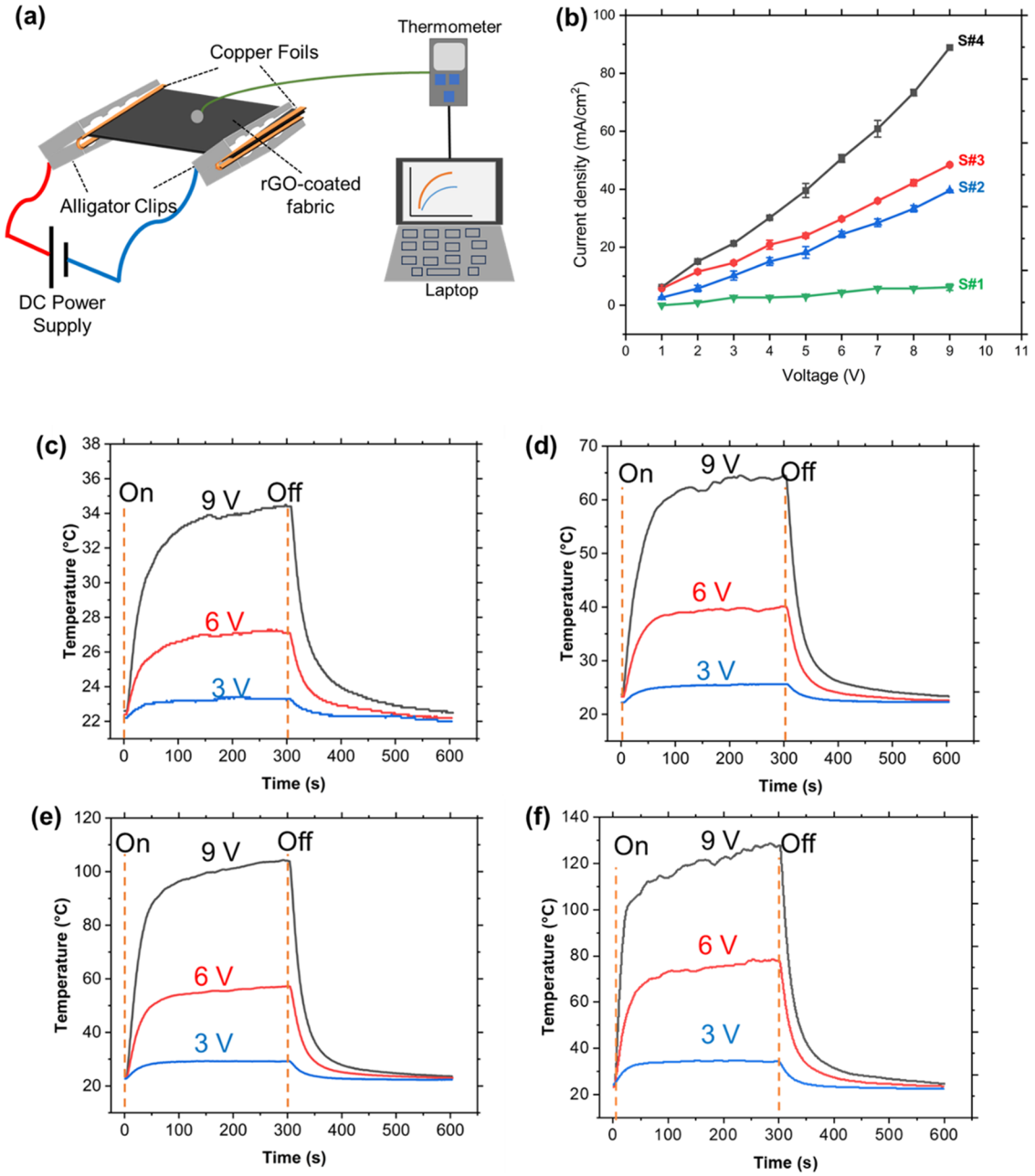

Figure 4. (a) Schematic representation of the experimental setup for electrothermal evaluation. (b) *V*–*I* curves for samples of varying rGO loading under different DC voltages. (c–f) Temperature profiles vs time under different applied voltages for samples S#1 (c), S#2 (d), S#3 (e), and S#4 (f).

Figure 4(c–f). For each sample, three different voltages were applied for a duration of 300 s, indicated by the "on" state on the graphs, and then the voltage was turned off, indicated by the "off" state. The temperature during each step was continuously monitored and recorded.

https://doi.org/10.1021/acsanm.3c03825
ACS Appl. Nano Mater. 2023, 6, 20006–20017

It should be noted that the applied voltages used in this study are significantly lower than the safe voltage limit of 36 V for the human body.[30] Hence, the rGO-coated fabrics are suitable and safe for use in thermotherapy applications.

A similar time-dependent temperature profile is observed for samples S#1, S#2, S#3, and S#4. In each case, there is an initial rapid temperature increase, followed by a slower rate of increase until a stable temperature is reached. The heating rate during the first step and the maximum temperature achieved in the second step are crucial factors when considering the performance of Joule heaters. The heating rate reflects the speed at which the temperature of the system increases, and maximum temperature indicates a balance between the input power supplied to the system and the amount of heat lost from it.[31] The results revealed that the initial 20 s period exhibited a remarkably high heating rate for all samples. Furthermore, the heating rate during this stage was observed to increase with a higher rGO content of the fabric. For instance, at 9 V, the average heating rates during this time were determined to be 0.26, 0.66, 1.6, and 3.6 °C/s for S#1, S#2, S#3, and S#4, respectively. Another parameter that influenced the heating rate was the applied voltage. Decreasing the voltage resulted in a decrease in the heating rate. For instance, in the case of S#4, the heating rate decreased to 1.06 °C/s when the voltage was lowered to 6 V.

The highest temperature achieved is by S#4 at 9 V, which is around 127 °C. The maximum temperature of the rGO-coated fabrics increased with higher rGO loading. For instance, saturated temperatures achieved under 9 V for S#1, S#2, and S#3 are 34.4, 64.5, and 104 °C, respectively. As depicted in the graphs, higher voltages in each case led to higher attained temperatures. Based on the obtained results and depending on the specific application, desired temperature, and heating rate, an appropriate rGO loading and voltage can be selected. For instance, a temperature below 60 °C is considered suitable for applications in physical therapy.[16] In this regard, fabric sample S#2, which has a rGO loading of 533 $\mu g/cm^2$, can meet the specific temperature requirements for such applications.

Table 3 summarizes the results reported by other studies on the electrothermal performance of fabrics modified with graphene or graphene composites. In comparison to previous studies, the rGO-coated fabrics prepared in this study demonstrated an outstanding Joule-heating performance.

Table 3. Comparison of the Maximum Temperature Achieved by Graphene-Functionalized Joule Heaters

conductive material	temperature, °C	voltage, V	ref
reduced graphene oxide	127	9	this work
reduced graphene oxide/silver	220	18	30
graphene nanoplatelets/carbon nanotubes	42.7	12	32
graphene	75.2	10	33
graphene	54.8	50	34
few-layer graphene	95	15	35
graphene-based inks	100.8	10	36

The robust performance of the rGO-coated fabrics in this work can potentially be attributed to two factors. First, the continuous and uniform coating of rGO on the fabric led to good electron mobility and efficient heat transfer and distribution. Second, the complete reduction of graphene oxide nanoflakes resulted in higher electrical conductivity and enhanced Joule-heating capabilities.

To assess the repeatability of the Joule-heating effect in the fabric, a voltage of 9 V was repeatedly applied to sample S#4 for a duration of 60 s, followed by a cooling step. This cycle was repeated a total of 8 times. The resulting temperature profile, depicting the variations in temperature throughout the repeated cycles, is presented in Figure S2. As evident from the data, the maximum temperature achieved in the first cycle is 112.6 °C, and the temperatures observed in subsequent cycles are within 5% of this value. This demonstrates the high repeatability of the Joule-heating effect exhibited by the rGO-coated fabric.

Antibacterial Performance. It has been reported that the inactivation rate of microorganisms in response to an electric field is influenced by both the applied current density and the duration of exposure.[37] Therefore, in this section of the study, different exposure times were investigated under a constant current density as well as varying current densities with the same exposure time. This analysis aimed to explore the impact of these variables on the inactivation of microorganisms. To conduct the antibacterial tests and investigate the electrothermal antibacterial effect of the rGO-coated fabric, *B. subtilis*, a Gram-positive bacterium, was used unless stated otherwise. Gram-positive bacteria are recognized for their higher resistance to heat due to their rigid cell wall structure.[38]

Since sample S#4 demonstrated a superior Joule-heating performance, fabrics with four iterations of the rGO coating were prepared to conduct the antibacterial tests under an electric field. In the initial experiment, 9 V resulting in a current density of 88.9 mA/cm^2 was applied to the rGO-coated fabrics for various exposure times (30, 90, 180, and 300 s). Following the application of voltage to the fabrics, the plate count method was employed to determine the number of viable cells present on each fabric. It is important to mention that for each antibacterial test, a pristine fabric without voltage application was employed as a control in the experiment. Figure 5(a–e) displays the agar plates obtained from the plate count method corresponding to each exposure time along with the control.

As observed, the number of viable colonies decreases with increasing the application time of the voltage. The number of colonies on each agar plate was quantified, and the reduction percentage was calculated using eq 2. The temperature profile of the fabric surface for 300 s application of 9 V of the antibacterial test is depicted in Figure 5f, accompanied by the corresponding reduction rates calculated at each exposure time. Since the rGO-coated fabric was wet during the antibacterial test, lower temperatures with reduced heating rates were achieved compared to when 9 V was applied to the dry sample S#4 (Figure 4f). After 30 s of application of the current, the fabric temperature reached approximately 58 °C, leading to a significant reduction of around 98% in bacteria. Previous studies indicated that temperatures higher than 70 °C are typically required to effectively kill bacteria.[39] Considering the temperatures achieved within the initial 90 s range and the substantial reduction in the bacterial count, it can be inferred that the inactivation of bacteria on the fabric is not solely dependent on thermal effects. It is evident that the presence of electricity applied to the fabric also significantly contributes to bactericidal activity. According to Powell et al., one of the primary pathways for bacterial killing under an electric field

https://doi.org/10.1021/acsanm.3c03825
ACS Appl. Nano Mater. 2023, 6, 20006−20017

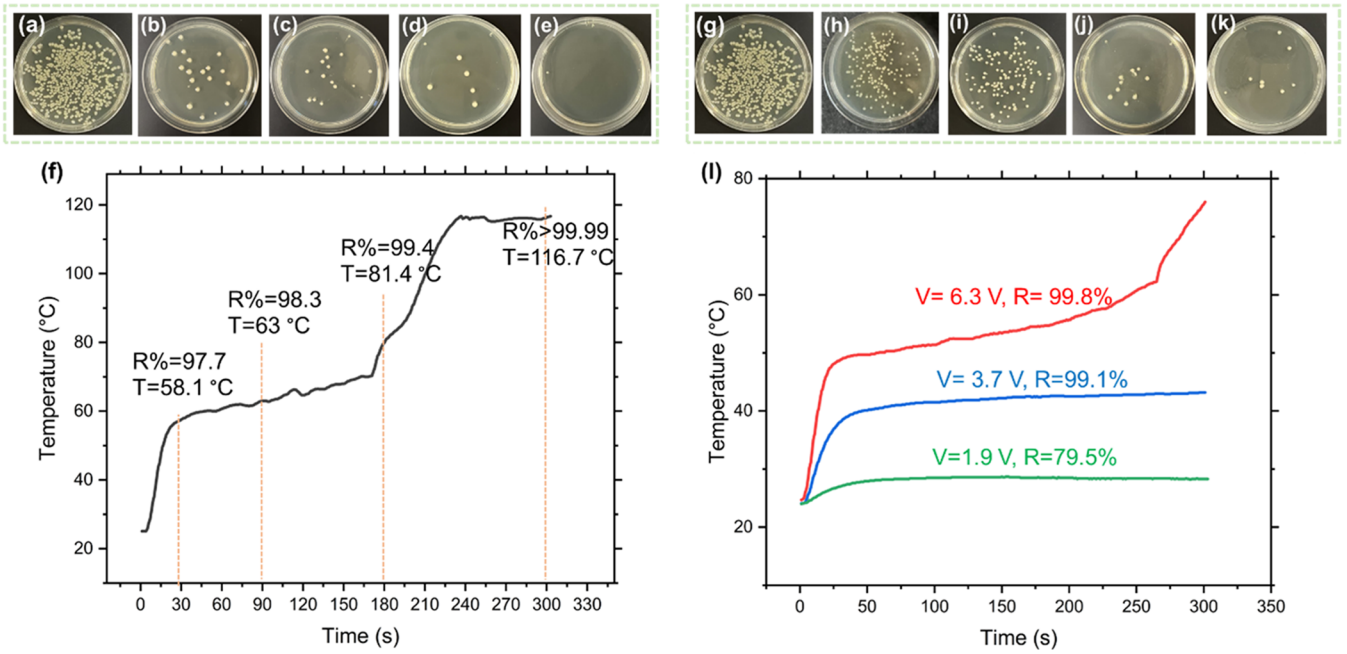

Figure 5. (a–e) Distribution of *B. subtilis* colonies on agar plates for (a) control and (b) 30 s, (c) 90 s, (d) 180 s, and (e) 300 s of 9 V application. (f) Temperature of the rGO-coated fabric vs time under 9 V during the antibacterial test and corresponding reduction percentage. (g–k) Distribution of *B. subtilis* colonies on agar plates under varying voltages: (g) control; (h) rGO-coated fabric, no voltage; (i) rGO-coated fabric, 1.9 V; (j) rGO-coated fabric, 3.7 V; and (k) rGO-coated fabric, 6.3 V. (l) Temperature profiles of different voltages applied to the fabric and the corresponding reduction percentage.

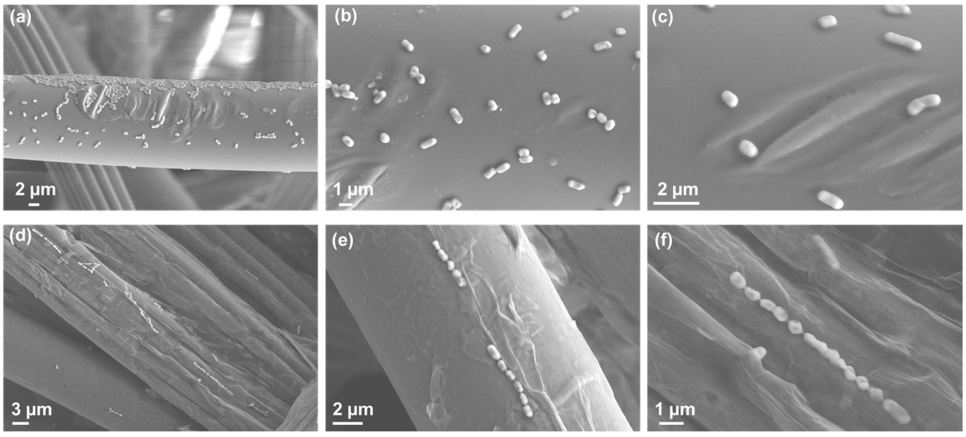

Figure 6. SEM images of *B. subtilis* cells on the control (a–c) and rGO-coated fabric after application of 9 V (d–f). The first column represents SEM images at 1840× magnification, while the second and third columns show 5210× and 8240× magnifications, respectively.

involves electron transfer between the conductive graphene-coated surface and bacteria.[13]

As the exposure time increased, higher temperatures were attained and the bacteria were subjected to electricity for a longer duration, leading to higher reduction rates. Ultimately, after 300 s of exposure, an exceptional reduction rate of over 99.99% was achieved for *B. subtilis* bacteria on the fabric, accompanied by a generated temperature of over 116 °C. This indicates that the thermal pathway likely played a more dominant role in the inactivation of the bacteria for this exposure time. Remarkably, this exceptional level of inactivation rate was achieved within a short contact time and with a power consumption of only 1.8 W. In contrast, conventional heating equipment typically requires several thousand W of power for the thermal removal of bacteria.

Following that, the antibacterial performance was assessed under voltages of 1.9, 3.7, and 6.3 V corresponding to current density levels of 22, 44, and 66 mA/cm^2, with a uniform exposure time of 300 s. Figure 5(g–k) shows the agar plates demonstrating the number of recovered colonies after each test. As expected, lower voltages resulting in lower current densities correspond to lower rates of bacterial removal. The rGO-coated fabric, when not subjected to current, demonstrates approximately 72% bacterial inactivation. This can be attributed to physical damage caused by the sharp edges and wrinkles of the rGO nanosheets to the bacterial cells as well as oxidative stress induced by rGO.[40]

Figure 5l presents temperature profiles during the antibacterial test corresponding to the applied voltage, along with the reduction rate. When an applied voltage of 1.9 V was utilized, the reduction rate did not demonstrate significant

https://doi.org/10.1021/acsanm.3c03825
ACS Appl. Nano Mater. 2023, 6, 20006–20017

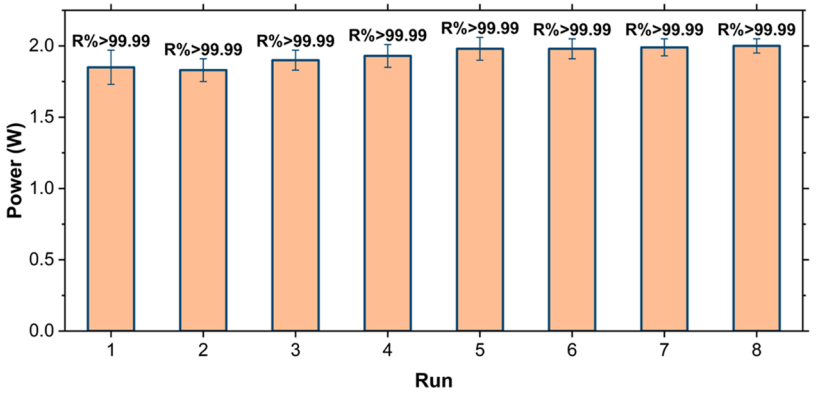

Figure 7. Repeatability of the antibacterial performance of the rGO-coated fabric under 9 V. The graph displays the power consumed during each run and the reduction rate (R%) against *B. subtilis*.

changes compared to when no voltage was applied. This can be ascribed to the fact that the electricity generated was not sufficient to cause membrane and physical damage to the bacterial cells. Additionally, with reference to the temperature profiles depicted in Figure 5l, it can be observed that the temperature of the fabric did not undergo a considerable increase that would induce thermal effects on the bacterial cells.

When a voltage of 3.7 V was applied, the temperature reached was still insufficient to cause bacterial cell death. However, a significant reduction rate of 99.1% was observed, which can be attributed to the electrical effects on the bacterial cells. These findings strongly indicate that the electrical effects play a pivotal role in the inactivation of the bacteria. Subsequently, a higher voltage of 6.3 V was tested, resulting in a higher current density and more elevated temperatures and consequently a higher reduction rate. In this case, both thermal and electrical mechanisms contribute to the bactericidal effect.

To visualize the impact of the electric field on bacterial cells, SEM images were captured from two samples: the control group (pristine fabric without current) and the rGO-coated fabric subjected to a voltage of 9 V for 300 s. These images, taken at various magnifications, are presented in Figure 6.

The SEM images demonstrate a noticeable distinction between the bacterial cells on the control sample and those on the rGO-coated fabric. In the control sample, the bacteria cells exhibit an intact rod-shaped morphology, indicating their preserved viability. Conversely, the bacterial cells on the rGO-coated fabric appear to have undergone a significant alteration in their original shapes, further confirming the loss of their viability due to the applied electric field.

The SEM images reveal a fascinating phenomenon in which the bacterial cells were aligned on the rGO-coated fabric in response to the electric field. The movement and orientation of cells induced by electrical stimuli hold significant potential for various applications, such as wound healing technologies and cancer therapy.[41,42]

Ensuring the repeatability of the rGO-coated fabric for antibacterial applications is of the utmost importance. To assess this aspect, multiple antibacterial tests were conducted on the fabric, involving a range of runs from 1 to 8, under an electric field. In each run, the voltage was adjusted to achieve a current density of 88.9 mA/cm^2 for a duration of 300 s. This specific combination of current density and exposure time was determined based on its ability to yield a reduction rate exceeding 99.99%. The reduction percentage and the power consumed were measured at each step, and the results are illustrated in Figure 7. Remarkably, the reduction rate of bacteria did not decrease even after 8 runs, indicating that the antibacterial efficacy of the rGO-coated fabric remains consistent and stable over multiple cycles of use. Additionally, the power consumption exhibited only a slight increase throughout the runs, suggesting that the energy requirements for achieving the desired antibacterial effect remain relatively low and do not significantly escalate with repeated use. These findings highlight the promising repeatability and efficient performance of the rGO-coated fabric for antibacterial applications.

Proposed Antibacterial Mechanism. Based on the observations made, it is plausible to suggest three main mechanisms that contribute to the bacterial inactivation on the rGO-coated fabric under an electric field

(1) Physical contact and chemical interaction with rGO nanosheets on the fabric's surface can lead to cell disruption. The sharp edges and wrinkles of the rGO nanosheets can physically disrupt the bacterial cell membranes, compromising their integrity.[43] Moreover, rGO nanosheets have the potential to induce oxidative stress through the generation of reactive oxygen species (ROS), resulting in bacterial DNA damage and inhibition of bacterial growth.[44] Previous studies have suggested that graphene materials can mediate the generation of ROS through the adsorption of O_2 on their defect sites and edges and subsequent reduction to ROS such as the superoxide radical (O^{2-}), the hydroxyl radical (OH), and hydrogen peroxide (H_2O_2).[45,46] Further experiments are required to carefully assess whether ROS is generated in this case and to evaluate their potential role in cell death, which will be a focus of our forthcoming research.

(2) Joule heat generated by the applied electric current can cause membrane damage, protein denaturation, DNA impairment, and enzyme inactivation within the bacterial cells.[47,48] The temperature is a critical environmental factor capable of significantly impacting the physiology of living cells.[49] For instance, reports indicate that temperatures around 50 °C lead to protein denaturation, while temperatures around 70 °C result in DNA melting.[50] Elevated temperatures beyond the optimal range for enzymes result in their denaturation and subsequent loss of activity.[51] Furthermore, high temper-

https://doi.org/10.1021/acsanm.3c03825
ACS Appl. Nano Mater. 2023, 6, 20006−20017

atures induce the fluidization of the cell membrane, potentially resulting in the breakdown of the lipid bilayer.[52] Fluidization refers to the increase in the mobility of lipid molecules within the membrane, disturbing the membrane's permeability[53] and potentially interfering with the transport and diffusion of biological materials.[54] Therefore, the increase in temperature resulting from Joule heating can lead to structural changes and functional impairment of cellular components.

(3) Electrical effects directly impact the bacterial cells through electroporation and direct electron transfer. These mechanisms result in destruction of the cell membrane, protein denaturation, and oxidation of enzymes.[12,55,56] It should be explained that electroporation refers to the formation of pores in the cell membrane induced by an external electric field.[57] These pores allow micro- and macromolecules to flow in and out of the cell,[58] leading to the disruption of the intracellular environment and eventual bacterial death.[59] Considering this, the electric field can induce disruptive forces on the cell membranes, rendering them permeable and susceptible to damage compromising the bacterial cell's viability.

These three pathways, namely, physical contact and chemical interaction with rGO, Joule-heating, and electrical effects, potentially contribute to the inactivation of bacteria on the rGO-coated fabric. In our future study, we will conduct distinct assessments to delve into each of these effects in detail to better understand them.

Antibacterial Effect on Gram-Negative Bacteria. Finally, a DC voltage of 9 V was applied to the rGO-coated fabric inoculated with *E. coli* bacteria for 300 s, which resulted in over a 99.99% reduction rate. Figure S3 demonstrates photographs of colonies recovered from the control and rGO-coated fabric. As can be observed, the control has numerous *E. coli* colonies, while no colonies were recovered after the application of electricity to the rGO-coated fabric. Therefore, the electrothermal treatment is effective for both Gram-positive and Gram-negative bacteria.

CONCLUSIONS

In summary, this study successfully demonstrated a method for fabricating rGO-coated fabrics with varying loading levels by using a simple in situ process. The resulting rGO-coated modified fabrics exhibit excellent Joule-heating capabilities under low voltages making them suitable for various applications such as thermotherapy. It was shown that increasing the rGO loading of the fabric resulted in a more continuous electron pathway. This, in turn, led to better electrical conductivity and enhanced electrothermal performance of the fabric. Furthermore, the rGO-coated fabrics showed remarkable antibacterial performance achieving significant reduction rates against both Gram-positive and Gram-negative bacteria. Three main mechanisms were proposed to account for the antibacterial performance of the rGO-coated fabrics: physical and chemical interactions of bacteria with rGO nanosheets, thermal effects resulting from Joule heating, and electrical effects. The combination of the Joule-heating effect and antibacterial properties makes the rGO-coated fabrics a valuable material for advanced applications in areas such as thermal management, personal protective equipment, and wound care. The fabric's ability to be used repeatedly not only ensures cost-effectiveness but also minimizes waste, promoting environmental sustainability.

ASSOCIATED CONTENT

Supporting Information

The Supporting Information is available free of charge at https://pubs.acs.org/doi/10.1021/acsanm.3c03825.

Additional details on experimental setup; *E. coli* test inoculum preparation procedure; and the preparation procedure of bacteria cells for SEM (PDF)

AUTHOR INFORMATION

Corresponding Author

Gerardine G. Botte − *Institute for Sustainability and Circular Economy, Chemical and Electrochemical Technology and Innovation Laboratory, Department of Chemical Engineering, Texas Tech University, Lubbock, Texas 79401, United States;* orcid.org/0000-0002-5678-6669; Phone: 806-834-8187; Email: gerri.botte@ttu.edu

Author

Behnaz Jafari − *Institute for Sustainability and Circular Economy, Chemical and Electrochemical Technology and Innovation Laboratory, Department of Chemical Engineering, Texas Tech University, Lubbock, Texas 79401, United States*

Complete contact information is available at: https://pubs.acs.org/10.1021/acsanm.3c03825

Notes

The authors declare the following competing financial interest(s): TEXAS TECH UNIVERSITY has recently filed a patent application arising from this work, where author G.G.B. is inventor, U.S. Patent Application No. 63/519,241 (2023).

ACKNOWLEDGMENTS

This work was funded by the National Science Foundation, EEC Division of Engineering Education and Centers, NSF Engineering Research Center for Advancing Sustainable and Distributed Fertilizer production (CASFER), NSF 20-553 Gen-4 Engineering Research Centers award # 2133576, the Chemical and Electrochemical Technology and Innovation (CETI) laboratory, and the Whitacre Department Chair Chemical Engineering, Texas Tech University.

REFERENCES

(1) Cho, S.; Chang, T.; Yu, T.; Lee, C. H. Smart electronic textiles for wearable sensing and display. *Biosensors* **2022**, *12* (4), No. 222, DOI: 10.3390/bios12040222.

(2) Guo, F.; Bao, Y.; Mao, J.; Xie, Y.; Huang, J.; Hu, X.; Lai, Y. Carboxyl Graphene Oxide Functionalized Cotton Textile with Superwettable Patterns for Humidity Sensing. *ACS Appl. Nano Mater.* **2022**, *6*, 261−269, DOI: 10.1021/acsanm.2c04343.

(3) Wang, C.; Xu, Q.; Hu, J.; Lu, P.; Wu, H.; Guo, B.; Tu, R.; Liu, K.; Yang, M.; Zhang, S.; et al. Graphene/SiC-coated textiles with excellent electromagnetic interference shielding, Joule heating, high-temperature resistance, and pressure-sensing performances. *J. Adv. Ceram.* **2023**, *12* (4), 778−791, DOI: 10.26599/JAC.2023.9220719.

(4) Zhang, Y.; Ren, H.; Chen, H.; Chen, Q.; Jin, L.; Peng, W.; Xin, S.; Bai, Y. Cotton fabrics decorated with conductive graphene nanosheet inks for flexible wearable heaters and strain sensors. *ACS Appl. Nano Mater.* **2021**, *4* (9), 9709−9720.

(5) Jalil, M. A.; Ahmed, A.; Hossain, M. M.; Adak, B.; Islam, M. T.; Moniruzzaman, M.; Parvez, M. S.; Shkir, M.; Mukhopadhyay, S. Synthesis of PEDOT: PSS Solution-Processed Electronic Textiles for Enhanced Joule Heating. *ACS Omega* **2022**, *7* (15), 12716−12723.
(6) Guo, Z.; Wang, Y.; Huang, J.; Zhang, S.; Zhang, R.; Ye, D.; Cai, G.; Yang, H.; Gu, S.; Xu, W. Multi-functional and water-resistant conductive silver nanoparticle-decorated cotton textiles with excellent joule heating performances and human motion monitoring. *Cellulose* **2021**, *28* (11), 7483−7495.
(7) Zhang, Y.; Jiang, Y.; Ge, F.; Li, Y. Improved electrothermal performance of graphene-carbon nanotubes composite films utilizing AgNWs coating method. *Flexible Printed Electron.* **2023**, *8* (1), No. 014001.
(8) Chaturvedi, M.; Patel, M.; Bisht, N.; Shruti; Mukherjee, M. D.; Tiwari, A.; Mondal, D.; Srivastava, A. K.; Dwivedi, N.; Dhand, C. Reduced Graphene Oxide-Polydopamine-Gold Nanoparticles: A Ternary Nanocomposite-Based Electrochemical Genosensor for Rapid and Early Mycobacterium tuberculosis Detection. *Biosensors* **2023**, *13* (3), No. 342, DOI: 10.3390/bios13030342.
(9) Zhang, F.; Yang, K.; Liu, G.; Chen, Y.; Wang, M.; Li, S.; Li, R. Recent Advances on Graphene: Synthesis, properties and applications. *Composites, Part A* **2022**, *160*, No. 107051, DOI: 10.1016/j.compositesa.2022.107051.
(10) Pandit, S.; Gaska, K.; Kádár, R.; Mijakovic, I. Graphene-based antimicrobial biomedical surfaces. *ChemPhysChem* **2021**, *22* (3), 250−263.
(11) Bhattacharjee, S.; Joshi, R.; Chughtai, A. A.; Macintyre, C. R. Graphene modified multifunctional personal protective clothing. *Adv. Mater. Interfaces* **2019**, *6* (21), No. 1900622.
(12) Barbhuiya, N. H.; Singh, S. P.; Makovitzki, A.; Narkhede, P.; Oren, Z.; Adar, Y.; Lupu, E.; Cherry, L.; Monash, A.; Arnusch, C. J. Virus inactivation in water using laser-induced graphene filters. *Materials* **2021**, *14* (12), No. 3179, DOI: 10.3390/ma14123179.
(13) Powell, C. D.; Pisharody, L.; Jopp, J.; Sharon-Gojman, R.; Tesfahunegn, B. A.; Arnusch, C. J. Laser-Induced Graphene Capacitive Killing of Bacteria. *ACS Appl. Bio Mater.* **2023**, *6* (2), 883−890, DOI: 10.1021/acsabm.2c01034.
(14) Li, K.; Zhang, Y.; Wang, Z.; Liu, L.; Liu, H.; Wang, J. Electrothermally driven membrane distillation for low-energy consumption and wetting mitigation. *Environ. Sci. Technol.* **2019**, *53* (22), 13506−13513.
(15) Heo, K. J.; Lee, Y.; Kim, S. B.; Kim, Y.-J.; Han, B.; Kim, H.-J. The Electro-Thermal Antimicrobial Carbon Surface. *IEEE Trans. Ind. Appl.* **2023**, *59* (1), 473−478.
(16) Hao, Y.; Tian, M.; Zhao, H.; Qu, L.; Zhu, S.; Zhang, X.; Chen, S.; Wang, K.; Ran, J. High efficiency electrothermal graphene/tourmaline composite fabric joule heater with durable abrasion resistance via a spray coating route. *Ind. Eng. Chem. Res.* **2018**, *57* (40), 13437−13448.
(17) Ruiz-Calleja, T.; Calderón-Villajos, R.; Bonet-Aracil, M.; Bou-Belda, E.; Gisbert-Payá, J.; Jiménez-Suárez, A.; Prolongo, S. G. Thermoelectrical properties of graphene knife-coated cellulosic fabrics for defect monitoring in Joule-heated textiles. *J. Ind. Text.* **2022**, *51*, 8884S−8905S.
(18) Jain, V. K.; Chatterjee, A. Graphene Functionalized Cotton Nonwoven for Thermotherapy. *J. Nat. Fibers* **2022**, *19* (16), 12883−12895.
(19) Jafari, B.; Lacerda, C. M.; Botte, G. G. Facile Electrochemical Preparation of Hydrophobic Antibacterial Fabrics Using Reduced Graphene Oxide/Silver Nanoparticles. *ChemElectroChem* **2023**, *10*, No. e202201111.
(20) Yotprayoonsak, P.; Anusak, N.; Virtanen, J.; Kangas, V.; Promarak, V. Facile fabrication of flexible and conductive AuNP/DWCNT fabric with enhanced Joule heating efficiency via spray coating route. *Microelectron. Eng.* **2022**, *255*, No. 111718.
(21) Fan, Z.; Liu, B.; Wang, J.; Zhang, S.; Lin, Q.; Gong, P.; Ma, L.; Yang, S. A novel wound dressing based on Ag/graphene polymer hydrogel: effectively kill bacteria and accelerate wound healing. *Adv. Funct. Mater.* **2014**, *24* (25), 3933−3943.
(22) Topsoe, H. Geometric factors in four point resistivity measurement. *Bulletin* **1968**, *472* (13), No. 63.
(23) de O Pereira, M. L.; Grasseschi, D.; Toma, H. E. Photocatalytic activity of reduced graphene oxide−gold nanoparticle nanomaterials: interaction with asphaltene and conversion of a model compound. *Energy Fuels* **2018**, *32* (3), 2673−2680, DOI: 10.1021/acs.energyfuels.7b02715.
(24) Koçanalı, A.; Varol, E. A. An experimental study on the electrical and thermal performance of reduced graphene oxide coated cotton fabric. *Int. J. Energy Res.* **2021**, *45* (9), 12915−12927, DOI: 10.1002/er.6623.
(25) Zeng, F.; Pan, D.; Pan, N. Choosing the impregnants by thermogravimetric analysis for preparing rayon-based carbon fibers. *J. Inorg. Organomet. Polym. Mater.* **2005**, *15*, 261−267.
(26) Teh, P.; Ng, H.; Yeoh, C. Recycled copper as the conductive filler in polyester composites. *Malays. Polym. J.* **2011**, *6* (1), 98−108.
(27) Bhattacharjee, S.; Macintyre, C. R.; Wen, X.; Bahl, P.; Kumar, U.; Chughtai, A. A.; Joshi, R. Nanoparticles incorporated graphene-based durable cotton fabrics. *Carbon* **2020**, *166*, 148−163.
(28) Ahmed, A.; Jalil, M. A.; Hossain, M. M.; Moniruzzaman, M.; Adak, B.; Islam, M. T.; Parvez, M. S.; Mukhopadhyay, S. A PEDOT: PSS and graphene-clad smart textile-based wearable electronic Joule heater with high thermal stability. *J. Mater. Chem. C* **2020**, *8* (45), 16204−16215.
(29) He, S.; Xin, B.; Chen, Z.; Liu, Y. Functionalization of cotton by reduced graphene oxide for improved electrical conductivity. *Text. Res. J.* **2019**, *89* (6), 1038−1050.
(30) Lin, S.-Y.; Zhang, T.-Y.; Lu, Q.; Wang, D.-Y.; Yang, Y.; Wu, X.-M.; Ren, T.-L. High-performance graphene-based flexible heater for wearable applications. *RSC Adv.* **2017**, *7* (43), 27001−27006.
(31) Bae, J. J.; Lim, S. C.; Han, G. H.; Jo, Y. W.; Doung, D. L.; Kim, E. S.; Chae, S. J.; Huy, T. Q.; Van Luan, N.; Lee, Y. H. Heat dissipation of transparent graphene defoggers. *Adv. Funct. Mater.* **2012**, *22* (22), 4819−4826.
(32) Sanivada, U. K.; Esteves, D.; Arruda, L. M.; Silva, C. A.; Moreira, I. P.; Fangueiro, R. Joule-heating effect of thin films with carbon-based nanomaterials. *Materials* **2022**, *15* (12), No. 4323, DOI: 10.3390/ma15124323.
(33) Tian, S.; He, P.; Chen, L.; Wang, H.; Ding, G.; Xie, X. Electrochemical fabrication of high quality graphene in mixed electrolyte for ultrafast electrothermal heater. *Chem. Mater.* **2017**, *29* (15), 6214−6219.
(34) Kim, H.; Lee, S.; Kim, H. Electrical heating performance of electro-conductive para-aramid knit manufactured by dip-coating in a graphene/waterborne polyurethane composite. *Sci. Rep.* **2019**, *9* (1), No. 1511.
(35) Ba, H.; Truong-Phuoc, L.; Papaefthimiou, V.; Sutter, C.; Pronkin, S.; Bahouka, A.; Lafue, Y.; Nguyen-Dinh, L.; Giambastiani, G.; Pham-Huu, C. Cotton fabrics coated with few-layer graphene as highly responsive surface heaters and integrated lightweight electronic-textile circuits. *ACS Appl. Nano Mater.* **2020**, *3* (10), 9771−9783.
(36) Karim, N.; Zhang, M.; Afroj, S.; Koncherry, V.; Potluri, P.; Novoselov, K. S. Graphene-based surface heater for de-icing applications. *RSC Adv.* **2018**, *8* (30), 16815−16823.
(37) Chiu, C.-M.; Ke, Y.-Y.; Chou, T.-M.; Lin, Y.-J.; Yang, P.-K.; Wu, C.-C.; Lin, Z.-H. Self-powered active antibacterial clothing through hybrid effects of nanowire-enhanced electric field electroporation and controllable hydrogen peroxide generation. *Nano Energy* **2018**, *53*, 1−10.
(38) Jung, J. H.; Lee, J. E.; Kim, S. S. Thermal effects on bacterial bioaerosols in continuous air flow. *Sci. Total Environ.* **2009**, *407* (16), 4723−4730.
(39) Shan, X.; Zhang, H.; Liu, C.; Yu, L.; Di, Y.; Zhang, X.; Dong, L.; Gan, Z. Reusable self-sterilization masks based on electrothermal graphene filters. *ACS Appl. Mater. Interfaces* **2020**, *12* (50), 56579−56586.
(40) Zou, F.; Zhou, H.; Jeong, D. Y.; Kwon, J.; Eom, S. U.; Park, T. J.; Hong, S. W.; Lee, J. Wrinkled surface-mediated antibacterial

activity of graphene oxide nanosheets. *ACS Appl. Mater. Interfaces* **2017**, *9* (2), 1343−1351.
(41) Tai, G.; Reid, B.; Cao, L.; Zhao, M. Electrotaxis and Wound Healing: Experimental Methods to Study Electric Fields as a Directional Signal for Cell Migration. In *Chemotaxis: Methods and Protocols*; Springer, 2009; Vol. *571*, pp 77−97.
(42) Cortese, B.; Palamà, I. E.; D'Amone, S.; Gigli, G. Influence of electrotaxis on cell behaviour. *Integr. Biol.* **2014**, *6* (9), 817−830.
(43) Makowski, T.; Svyntkivska, M.; Piorkowska, E.; Mizerska, U.; Fortuniak, W.; Kowalczyk, D.; Brzezinski, S.; Kregiel, D. Antibacterial electroconductive composite coating of cotton fabric. *Materials* **2022**, *15* (3), No. 1072, DOI: 10.3390/ma15031072.
(44) Cao, G.; Yan, J.; Ning, X.; Zhang, Q.; Wu, Q.; Bi, L.; Zhang, Y.; Han, Y.; Guo, J. Antibacterial and antibiofilm properties of graphene and its derivatives. *Colloids Surf., B* **2021**, *200*, No. 111588.
(45) Gurunathan, S.; Han, J. W.; Dayem, A. A.; Eppakayala, V.; Kim, J.-H. Oxidative stress-mediated antibacterial activity of graphene oxide and reduced graphene oxide in Pseudomonas aeruginosa. *Int. J. Nanomed.* **2012**, 5901−5914.
(46) Zou, X.; Zhang, L.; Wang, Z.; Luo, Y. Mechanisms of the antimicrobial activities of graphene materials. *J. Am. Chem. Soc.* **2016**, *138* (7), 2064−2077.
(47) Russell, A. Lethal effects of heat on bacterial physiology and structure. *Sci. Prog.* **2003**, *86* (1−2), 115−137.
(48) Sharma, C. P.; Arnusch, C. J. Laser-induced graphene composite adhesive tape with electro-photo-thermal heating and antimicrobial capabilities. *Carbon* **2022**, *196*, 102−109.
(49) Leach, M. D.; Cowen, L. E. Membrane fluidity and temperature sensing are coupled via circuitry comprised of Ole1, Rsp5, and Hsf1 in Candida albicans. *Eukaryotic cell* **2014**, *13* (8), 1077−1084.
(50) Kotnik, T.; Frey, W.; Sack, M.; Meglič, S. H.; Peterka, M.; Miklavčič, D. Electroporation-based applications in biotechnology. *Trends Biotechnol.* **2015**, *33* (8), 480−488.
(51) Deeth, H. C. Heat-induced inactivation of enzymes in milk and dairy products. A review. *Int. Dairy J.* **2021**, *121*, No. 105104.
(52) Los, D. A.; Murata, N. Membrane fluidity and its roles in the perception of environmental signals. *Biochim. Biophys. Acta, Biomembr.* **2004**, *1666* (1−2), 142−157.
(53) Shigapova, N.; Török, Z.; Balogh, G.; Goloubinoff, P.; Vígh, L.; Horváth, I. Membrane fluidization triggers membrane remodeling which affects the thermotolerance in Escherichia coli. *Biochem. Biophys. Res. Commun.* **2005**, *328* (4), 1216−1223.
(54) Fonseca, F.; Pénicaud, C.; Tymczyszyn, E. E.; Gómez-Zavaglia, A.; Passot, S. Factors influencing the membrane fluidity and the impact on production of lactic acid bacteria starters. *Appl. Microbiol. Biotechnol.* **2019**, *103*, 6867−6883.
(55) Singh, S. P.; Li, Y.; Be'er, A.; Oren, Y.; Tour, J. M.; Arnusch, C. J. Laser-induced graphene layers and electrodes prevents microbial fouling and exerts antimicrobial action. *ACS Appl. Mater. Interfaces* **2017**, *9* (21), 18238−18247.
(56) Del Pozo, J. L.; Rouse, M. S.; Mandrekar, J. N.; Steckelberg, J. M.; Patel, R. The electricidal effect: reduction of Staphylococcus and Pseudomonas biofilms by prolonged exposure to low-intensity electrical current. *Antimicrob. Agents Chemother.* **2009**, *53* (1), 41−45.
(57) Tieleman, D. P. The molecular basis of electroporation. *BMC Biochem.* **2004**, *5*, No. 10, DOI: 10.1186/1471-2091-5-10.
(58) Korem, M.; Goldberg, N.; Cahan, A.; Cohen, M.; Nissenbaum, I.; Moses, A. Clinically applicable irreversible electroporation for eradication of micro-organisms. *Lett. Appl. Microbiol.* **2018**, *67* (1), 15−21.
(59) Liu, C.; Xie, X.; Zhao, W.; Liu, N.; Maraccini, P. A.; Sassoubre, L. M.; Boehm, A. B.; Cui, Y. Conducting nanosponge electroporation for affordable and high-efficiency disinfection of bacteria and viruses in water. *Nano Lett.* **2013**, *13* (9), 4288−4293.

https://doi.org/10.1021/acsanm.3c03825
ACS Appl. Nano Mater. 2023, 6, 20006−20017